

## STRUCTURAL PERFORMANCE OF MARINE CIRCULAR REINFORCED CONCRETE PIERS UNDER AXIAL LOADING

M. A. Hajiyev<sup>\*1</sup>, I. G. Huseynov<sup>2</sup>, U. M. Hajiyeva<sup>3</sup>, S. R. Bashirzade<sup>1</sup>

<sup>1</sup>Azerbaijan University of Architecture and Construction, Baku, Azerbaijan

<sup>2</sup>Azerbaijan State University of Oil and Industry, Baku, Azerbaijan

<sup>3</sup>«OilGasScientificResearchProject» Institute, SOCAR, Baku, Azerbaijan

### ABSTRACT

In this study, an analytical framework was developed for the analysis of the structural behavior of marine circular RC piers under axial compressive loads, accounting for material and geometric nonlinearities. The proposed methodology includes the biaxial stress-strain relationships of concrete and reinforcement within the anisotropic behavior that these materials exhibit under loads. With this type of methodology, it is possible to model critical factors such as concrete cracking, reinforcement yielding, and material interactions. In addition, geometric influences, including slenderness and stability, were analyzed to properly understand pier performance. A parametric study was extended to the influence of the main design parameters, namely, concrete compressive strength, pier height, and reinforcement ratio. Indeed, higher classes of concrete strength provide an important increase in the load-bearing capacity and improvement in structural behavior. The same trends were observed with respect to the variation in pier height, which directly affects the slenderness ratios and stability parameters, indicating geometrical dimensioning optimization in the process of structural design. The reinforcement ratio has a positive effect on the critical stress distribution and enhancement of the critical load capacity. Subsequently, a series of FEA using the DIANA program was performed to verify the analytical framework. As a result, all the FEA results featured by good correspondences against such an analytical prediction are provided in proving the effectiveness of the proposed method with a sufficient degree of precision. This alignment underlines the effectiveness of the analytical approach for understanding the complex behavior of RC piers subjected to axial compression.

**Keywords:** marine structures; offshore structures; circular reinforced concrete piers; axial compression; slenderness; finite element analysis (FEA); load-bearing capacity; stability.

**Date submitted:** 06.01.2025

**Date accepted:** 05.05.2025

© 2025 «OilGasScientificResearchProject» Institute. All rights reserved.

### 1. Introduction

Marine structures, especially those made of reinforced concrete piers with circular cross sections, play a very important role in supporting infrastructure located in both coastal and offshore areas. These structures could be subjected to various loading conditions. In this regard, the durability and performance of reinforced concrete piers in marine environments are of prime importance from the viewpoint of structural integrity and service life. Circular reinforced concrete (RC) piers are among the most important structural members and are widely applied in primary structures in many engineering fields, including bridges, buildings, and marine structures. Their popularity is due to a number of advantageous features such as ease of construction and high load-carrying capacity. Owing to these properties, they are particularly suited for vertical load-carrying purposes under difficult structural circumstances, with good efficiency and reliability.

The analysis and prediction of the load-carrying capacity of circular RC columns are significantly more complex than those of rectangular RC columns. Such complications arise because of the peculiarities of the geometric configurations, stress distributions, and failure mechanisms related to their circular cross-sections. Indeed, it was underlined in previous studies [1, 2] that the peculiar structural behavior of circular RC columns requires more sophisticated approaches for accurate capacity estimation. To solve these problems, many researchers have developed effective and simplified methods for predicting the structural resistance of uncorroded circular RC columns. In such methods, computational efficiency must be balanced with predictive accuracy to enable engineers to check structural safety and performance under different load conditions. The most valuable contributions in this area have been provided [2, 3].

Various studies in this field provide general information about the behavior of such structures. Their behavior under seismic loads has been studied on RC columns and bridge piers based on strengthening techniques and mate-

\*E-mail: [hajiyevmuxlis@mail.ru](mailto:hajiyevmuxlis@mail.ru)

<http://dx.doi.org/10.5510/OGP20250201073>

rial properties. Image processing to observe thin cracks in an RC bridge pier demonstrates the potential of advanced techniques for structural health monitoring [4]. Laboratory tests and numerical simulations of barge impacts on circular RC piers [5] have analyzed the degree of reinforcement and concrete strength affecting the seismic performance, and how different material selections affect the structural behavior during earthquakes has been presented. The compressive strength related to the improvement in the structural capacity of hybrid concrete-steel systems has been investigated for circular concrete-filled steel pipe columns [6, 7].

A study investigated the inelastic behavior and ductility capacity of circular hollow RC bridge piers under seismic conditions to provide a better design for earthquake resistance [8]. The axial load axial deformation behavior of circular concrete columns reinforced with GFRP bars and helices has been investigated, and this may provide insight into alternative strengthening materials available to improve column performance [9].

In the reliability-based capacity design of reinforced concrete bridge structures, the view that safety should be guaranteed through the design of the structure [10] has been proposed, and the reinforcement of the concrete column with square reinforcement for circularization and FRP confinement has provided an effective strengthening method to improve column strength. The cyclic behavior of FRP concrete bridge pier frames contributes to the improvement of knowledge regarding the dynamic load on a bridge structure [11, 12].

Axial crushing of circular columns has been investigated, and important data have been provided to improve the design of structures subjected to extreme loads [13]. The behavior of double-walled circular cantilevered columns filled with concrete under compression provides valuable insights into the design of tubular structures [14].

The stress-strain behavior of concrete in circular columns partially wrapped with FRP strips has contributed to the development of effective confinement techniques to improve column performance. Models for evaluating circular concrete columns confined with different FRP composites have advanced the understanding of the interaction between concrete and FRP materials in column behavior [15, 16]. Finally, experimental investigations on circular concrete columns reinforced with GFRP bars and helices under different loading conditions further support the practical application of GFRP reinforcement in concrete columns to improve strength and durability [17].

Recent studies have focused on the stress-strain state and bearing capacity of concrete elements represented by compressed reinforced concrete and pipe-concrete elements. An investigation was conducted on both the stress-strain condition and bearing capacity of axially compressed pipe-concrete elements and annular-section reinforced concrete elements, and important results were obtained with reference to their mechanical behavior and practical application [18, 19]. In addition, the getting of the «moment-curvature» diagram for RC elements has been investigated, and calculation methods for reinforced concrete beams have been advanced [20]. Further studies have been directed toward nonlinear deformation models for circular-section compressed reinforced concrete elements, providing novel insights into the stress-strain analysis approaches and

bearing capacities of such structures [21, 22]. In addition, the stress-strain behavior of circular-section compressed reinforced concrete elements was investigated based on two-axis diagrams of the material, which are important for effective structural design [23, 24].

In this study, analytical formulas were developed to evaluate the general performance of circular piers as support structures for marine structures. A methodology was developed to determine the stress deformation state and bearing capacity of circular section short-span RC elements under compression by applying a biaxial diagram to model the compression behavior of concrete. This methodology provides the opportunity to determine the bearing capacity regardless of the eccentricity of the compression force and the flexibility of the element. The developed analytical method has the potential to predict the behavior of piers in marine structures more accurately. To test the accuracy of this methodology, a comparison was made with the finite element method using the DIANA FEA program [32], and the reliability and validity of the results obtained using the analytical formulas were determined.

## 2. Problem statement

### 2.1. Theoretical background of the problem and analytical solution proposition

Compressed RC piers are among the most common load-bearing components used in marine constructions. RC piers are used as structural supports, and their cross-sectional shapes are typically circular. The geometric configuration is advantageous because it resists loads uniformly in all directions, making the circular sections highly efficient for load-bearing purposes. The geometry of the circular cross-section introduces complicated developments in simplified methodologies for engineering calculations. In most cases, it is not possible to develop simple formulas for these elements because of their complicated structural behavior. Thus, normative documents and design codes normally recommend analysis using approximate methods. Such recommendations represent a balance between computational simplicity and accuracy, enabling practical engineering solutions. On the other hand, modern structural design theories aim to optimize the exploitation of material strength reserves. The development of computational tools and advanced analytical procedures allows for more accurate modeling of stress-strain relationships with respect to the optimum performance and safety margins. The stress-strain behaviors of concrete (fig. 1a) and reinforcing steel (fig. 1b) in tension and compression are usually modeled using bilinear diagrams according to modern construction standards, which are more commonly known as two-axis stress-strain models [25, 26, 31]. These diagrams effectively and in a simplified form but representative-display material behavior that enables advanced numerical and analytical evaluations.

Stress-strain diagrams have been conventionally used for specifying the mechanical behavior of heavyweight concrete under short-term loading conditions. These diagrams can be applied with a better approximation for concrete with compressive strength classes not greater than B60. Some simplifying assumptions were valid for under mentioned class. For example, it could be assumed that  $\varepsilon_{b2}=0.0035$ , and hence, there is a direct proportionality between the

stress and strain within the elastic region. For heavyweight concrete, one may suggest that  $\epsilon_{b1}=0.0015$ ;  $\epsilon_{b0}=0.002$ ; and  $\sigma_{b1}=0.6 \cdot R_b$ . These equalities indicate the equivalence in behavior between different deformation zones within the performance limit of the material. Furthermore, the stress-strain diagram shows that stress  $\sigma$  is a function of deformation  $\epsilon$ . Considering the deformation value, the stress was determined using the following expression:

$$\sigma_b = \begin{cases} \frac{\sigma_{b1}}{\epsilon_{b1}} \cdot \epsilon_b; & \text{if } \epsilon_b < \epsilon_{b1} \\ R_b; & \text{if } \epsilon_b \geq \epsilon_{b1} \end{cases} \quad (1)$$

According to the section calculation of the considered RC element (fig. 2), when the plane section hypothesis is accepted for a complex section [18-23, 31], the distribution of the deformation over the height of the section can be written as

$$\epsilon_{bz} = \frac{\epsilon_b}{x} \cdot (x - R + z) \quad (2)$$

In this case, depending on the position of the neutral axis, the following equations can be written for the internal normal force and bending moment arising from the normal compressive stresses in the concrete in the section:

a) If  $\epsilon_b \leq \epsilon_{b1}$  (fig. 2a);

$$N_b(\epsilon_b, x) = 2 \cdot \frac{R_b}{\epsilon_{b1}} \cdot \frac{\epsilon_b}{x} \cdot \int_q^R (x - R + z) \cdot \sqrt{R^2 - z^2} dz \quad (3)$$

$$M_b(\epsilon_b, x) = 2 \cdot \frac{R_b}{\epsilon_{b1}} \cdot \frac{\epsilon_b}{x} \cdot \int_q^R (x - R + z) \cdot z \cdot \sqrt{R^2 - z^2} dz \quad (4)$$

According to the integral tables, if, it includes the following functions:

$$J(R, z) = \int \sqrt{R^2 - z^2} dz = \frac{R^2}{2} \cdot \arcsin\left(\frac{z}{R}\right) + \frac{z}{2} \cdot \sqrt{R^2 - z^2}$$

$$J_1(R, z) = \int z \cdot \sqrt{R^2 - z^2} dz = -\frac{1}{3} \cdot (R^2 - z^2) \cdot \sqrt{R^2 - z^2}$$

$$J_2(R, z) = \int z^2 \cdot \sqrt{R^2 - z^2} dz = \frac{R^4}{8} \cdot \arcsin\left(\frac{z}{R}\right) - \frac{R^2}{8} \cdot z \cdot \sqrt{R^2 - z^2} + \frac{z^3}{4} \cdot \sqrt{R^2 - z^2} \quad (5)$$

The integrals above can be expressed in a simpler manner as follows:

$$N_b(\epsilon_b, x) = 2 \cdot \frac{R_b}{\epsilon_{b1}} \cdot \frac{\epsilon_b}{x} \cdot (x - R) \cdot (J(R, R) - J(R, q)) + 2 \cdot \frac{R_b}{\epsilon_{b1}} \cdot \frac{\epsilon_b}{x} \cdot (J_1(R, R) - J_1(R, q)) \quad (6)$$

$$M_b(\epsilon_b, x) = 2 \cdot \frac{R_b}{\epsilon_{b1}} \cdot \frac{\epsilon_b}{x} \cdot (x - R) \cdot (J_2(R, R) - J_2(R, q)) + 2 \cdot \frac{R_b}{\epsilon_{b1}} \cdot \frac{\epsilon_b}{x} \cdot (J_2(R, R) - J_2(R, q)) \quad (7)$$

b) If  $\epsilon_b \geq \epsilon_{b1}$  (fig. 2b);

$$N_b(\epsilon_b, x) = 2 \cdot \frac{R_b}{\epsilon_{b1}} \cdot \frac{\epsilon_b}{x} \cdot \int_q^{z_A} (x - R + z) \cdot \sqrt{R^2 - z^2} dz + 2R_b \cdot \int_{z_A}^R \sqrt{R^2 - z^2} dz \quad (8)$$

$$M_b(\epsilon_b, x) = 2 \cdot \frac{R_b}{\epsilon_{b1}} \cdot \frac{\epsilon_b}{x} \cdot \int_q^{z_A} (x - R + z) \cdot z \cdot \sqrt{R^2 - z^2} dz + 2R_b \cdot \int_{z_A}^R z \cdot \sqrt{R^2 - z^2} dz \quad (9)$$

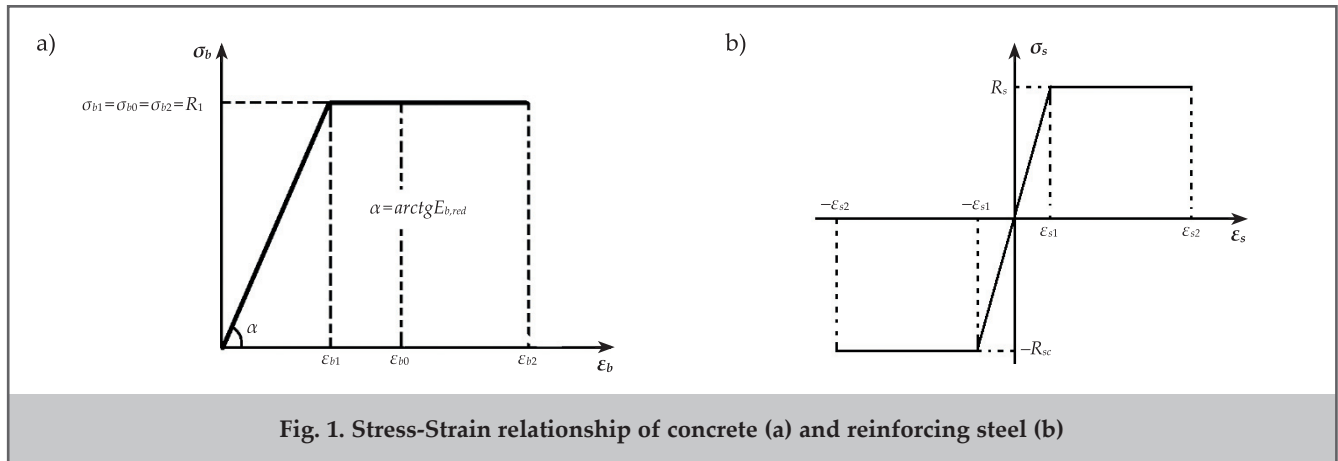


Fig. 1. Stress-Strain relationship of concrete (a) and reinforcing steel (b)

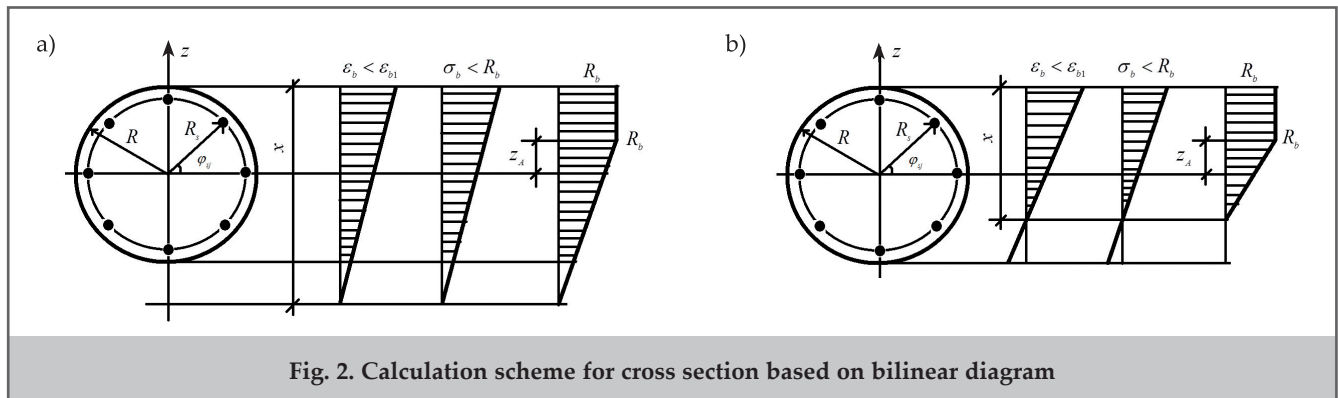


Fig. 2. Calculation scheme for cross section based on bilinear diagram

Considering the function (5) included here, (8) and (9) can be written for the internal force and moment as

$$N_b(\varepsilon_b, x) = 2 \cdot \frac{R_b}{\varepsilon_{b1}} \cdot \frac{\varepsilon_b}{x} \cdot (x - R) \cdot (J(R, z_A) - J(R, q)) + 2 \cdot \frac{R_b}{\varepsilon_{b1}} \cdot \frac{\varepsilon_b}{x} \cdot (J_1(R, z_A) - J_1(R, q)) + 2R_b \cdot (J(R, R) - J(R, z_A)) \quad (10)$$

$$M_b(\varepsilon_b, x) = 2 \cdot \frac{R_b}{\varepsilon_{b1}} \cdot \frac{\varepsilon_b}{x} \cdot (x - R) \cdot (J_1(R, z_A) - J_1(R, q)) + 2 \cdot \frac{R_b}{\varepsilon_{b1}} \cdot \frac{\varepsilon_b}{x} \cdot (J_2(R, z_A) - J_2(R, q)) + 2R_b \cdot (J_1(R, R) - J_1(R, z_A)) \quad (11)$$

According to figure 2 in the above equations;

$$q = \begin{cases} R - x, & \text{if } x < 2R \\ -R, & \text{if } x \geq 2R \end{cases} \quad \text{and} \quad z_A = \frac{\varepsilon_{b1}}{\varepsilon_b} \cdot x - x + R \quad (12)$$

$$\sigma_s = \begin{cases} \frac{R_s}{\varepsilon_{s1}} \cdot \varepsilon_s; & \text{if } |\varepsilon_s| < \varepsilon_{s1}; \\ R_s \cdot \varepsilon_s / |\varepsilon_s|; & \text{if } |\varepsilon_s| \geq \varepsilon_{s1} \end{cases} \quad (13)$$

Here, it is assumed that the reinforcement bars work similarly in tension and compression, that is,  $R_s = R_{sc}$ . If the total number of longitudinal reinforcement bars in the cross section is denoted by  $R_s$ , then according to figure 2, the deformation of the reinforcement bars can be written as

$$\varepsilon_{sj} = \frac{\varepsilon_b}{x} \cdot (x - R + R_{sj} \cdot \sin \varphi_{sj}), \quad j = 1, 2, \dots, k_s \quad (14)$$

The following equations can then be written for the internal normal force and bending moment arising in the section from the normal stresses in the reinforcement bars:

$$N_s(\varepsilon_b, x) = \sum_{j=1}^{k_s} \sigma_{sj} \cdot A_{sj} \quad (15)$$

$$N_s(\varepsilon_b, x) = \sum_{j=1}^{k_s} \sigma_{sj} \cdot A_{sj} \cdot R_{sj} \cdot \sin \varphi_{sj} \quad (16)$$

In these equations, the quantity  $A_{sj}$  is the cross-sectional area of the  $j$ -th reinforcement bar.

According to this calculation scheme, if we approximate the bent axis of the shaft as

$$y = f \cdot \sin \frac{\pi \cdot x}{2l} \quad (17),$$

the maximum deflection of the shaft can be expressed as  $f$ , the deformation of concrete on the compression face of the most stressed section  $\varepsilon_b$ , and the parameter  $x$ , which determines the position of the neutral axis in this section,

$$\rho^* = \frac{4l^2}{\pi^2} \quad (18)$$

where

$$f = \rho^* \cdot \frac{\varepsilon_b}{x} \quad (19)$$

Based on the above equations, the equilibrium equations of the support structure in compression on the most stressed section can be written as

$$\begin{aligned} N_b(\varepsilon_b, x) + N_s(\varepsilon_b, x) &= P, \\ M_b(\varepsilon_b, x) + M_s(\varepsilon_b, x) &= P \left( e + \rho^* \cdot \frac{\varepsilon_b}{x} \right) \end{aligned} \quad (20)$$

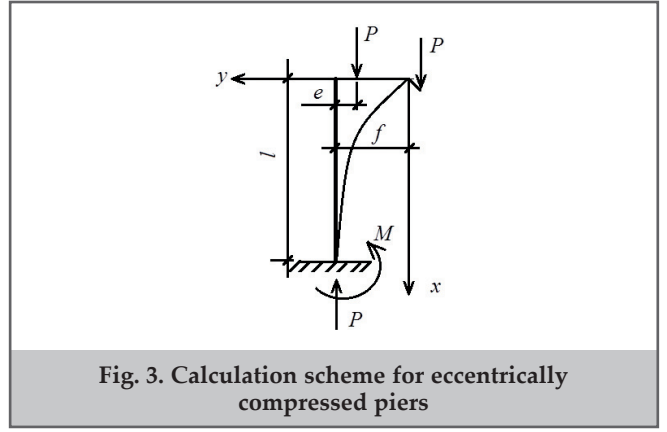


Fig. 3. Calculation scheme for eccentrically compressed piers

### 2.2. Solution of problem

Thus, the solution of the problem is reduced to the solution of a system of nonlinear equations in terms of parameters  $\varepsilon_b$  and  $x$ , which are the main parameters characterizing the state of stress-strain deformation in the most stressed section. After these two parameters are determined, the other parameters can be easily calculated. Because the obtained system was nonlinear, its analytical solution was not possible. The application of the semi-inverse method proposed in [18] to solve this system is effective. The essence of this method is that, based on the deformation diagram of concrete in compression, the interval of change of deformation  $\varepsilon_b$  is known in advance. Assuming the value of this parameter, the parameter corresponding to the accepted value of the deformation can be determined with any accuracy from the equation of the unknown obtained from Eq. (20).

$$\begin{aligned} \Psi(\varepsilon_b, x) &= M_b(\varepsilon_b, x) + M_s(\varepsilon_b, x) - \\ &- (N_b(\varepsilon_b, x) + N_s(\varepsilon_b, x)) \cdot \left( e + \rho^* \cdot \frac{\varepsilon_b}{x} \right) = 0 \end{aligned} \quad (21)$$

Subsequently, the value of the slope is determined based on (18), and finally, the value of the external compressive force  $P$  is determined based on the first equation of the system (20). Based on the described methodology,  $P \div f$  «load-displacement» curve can be easily constructed based on which the load-bearing capacity of the compressed element can be determined. In addition, based on Eqs. (13) and (14) obtained above, the stresses in the reinforcement bars can be determined at each solution step. This allows tracking of the nature of the changes in the stresses in the reinforcement rods depending on the loading level.

### 3. Parametric study

A corresponding software module was developed to apply the proposed analytical calculation algorithm, and various parametric studies were conducted using this module. The main objective of this study is to analyze the effects of different parameters on the performance of piers and to demonstrate the practical effectiveness of the proposed methodology. During this study, the elements were conditionally subjected to central compression. In addition, the value of the eccentricity of the compressive force was assumed to be equal to the value of the random eccentricity ( $e=0.01 m$ ), and the model was adapted to real structural conditions. In the analysis process, various variable parameters were considered, as shown in table 1. The strength of concrete at different values was analyzed, and the relative amount of reinforcement in

Details of parametric study			Table 1
Research parameters		Output of parametric study	Other design parameters of study
Concrete compressive strength:	B20, 11.5 MPa B30, 17.0 MPa B40, 22.0 MPa	<ul style="list-style-type: none"> <li>• Performance difference of piers for various concrete compressive strengths.</li> <li>• Position change in the neutral axis, depending on the deformation of the concrete.</li> <li>• The maximum normal force and bending moment changes generated in the concrete (<math>N_b</math>, <math>M_b</math>) and reinforced bar (<math>N_s</math>, <math>M_s</math>) in the most stressed section varied depending on the deformation of the compression face of the section.</li> <li>• Stress changes in the reinforcement bars during deformation in the most stressed part of the cross-section</li> </ul>	Pier radius: $R=0.3$ m Reinforced bar: $12\text{Ø}20$ $R_s = R_{sc} = 350$ MPa
Pier heights:	$l=2.0$ m $l=3.0$ m $l=5.0$ m		
Reinforcement ratio:	0.85% ( $12\text{Ø}16$ ) 1.61% ( $12\text{Ø}22$ ) 2.61% ( $12\text{Ø}28$ )		Pier radius: $R=0.3$ m Concrete: B30, $R_b=17.0$ MPa Pier height: $l=4.0$ m $R_s = R_{sc} = 350$ MPa

the concrete cross-section was taken as a variable parameter, considering the different heights of the pier. Different values were selected for each parameter, and the behavior of the structural elements under load was simulated.

#### 4. FE verification

A validation process was conducted to corroborate the accuracy and reliability of the proposed analytical methodology using one of the analyzed FE piers. Through this, the FE analysis simulated the mechanical behavior in piers with higher accuracy compared to methodologies related to quality assessment.

In the analysis, the dimensions and material properties of the pier were carefully selected and modeled according to the previous mentioned analytical method parameters. The total height of the pier was assumed to be 3 m, and the radius was 0.3 m. The material properties were taken as B30 class concrete and 350 MPa for the tensile strength of the reinforcement. During the design, 12 reinforcing bars, each with a diameter of 20 mm, were used to analyze the bearing capacity and mechanical behavior. These reinforcements were evenly distributed inside the pier, and an adherent-slip model was applied to ensure an effective adhesion with the concrete (fig. 4).

In the FE model, the concrete and embedded reinforcements were modelled using 3D solid elements. The cracking

behavior of concrete was described by a general deformation crack model, and its behavior up to the breaking point was studied by pushover analyses. The Hognestad curve was used to model the compression behavior of the concrete, and an exponential softening model was used for the tension [33, 34]. The behavior of the reinforcement elements was modeled together with the concrete based on the adherens-slip model, and linear plastic hardening based on von Mises plasticity was considered [34-36]. In the FE model, 3D solid elements (HX24L) were used, which allowed an accurate description of the complex geometry. Three degrees of freedom are provided for each node in the model. Both material and geometric nonlinearities were considered, and realistic features such as crack initiation and propagation, plasticity, and large deformation were included. The behavior of the scaffold under load was studied up to the point of failure through pushover analyses. Post-peak behavior was observed by successively increasing the point loads. The loads were applied in increments ranging from 1.0 to 5.0 kN, and this approach ensured both the stability and efficiency of the analysis process. In the FE analysis, the convergence criteria were strictly followed, and the main output parameters such as displacement and stress distribution were analyzed.

## 5. Results and discussion

### 5.1. Effect of concrete compressive strength (concrete class) on the structural performance of RC circular piers

This study comprehensively addressed the influence of the concrete compressive strength on the load-bearing capacity of a circular RC pier. As expected, the results showed a significant correlation between increasing the class of concrete and enhancing the structural performance (fig. 5). It was determined from the analysis that the maximum load for B20 class concrete was 3982.8 kN. Considering the B30 class concrete, the maximum load further increased to 5309 kN with an increase of 33.4% in the load-carrying capacity. In the case of the B40 class concrete, the maximum load is further increased to 6512.9 kN. This constitutes a further increase of 22.7% over and above the B30 class, and a total increase of 63.5% over the B20 class. It was determined that owing to the increase in class, some deformation indicators showed minor declines that helped to maintain the stability of piers at maximum load application. All classes have similar deformation

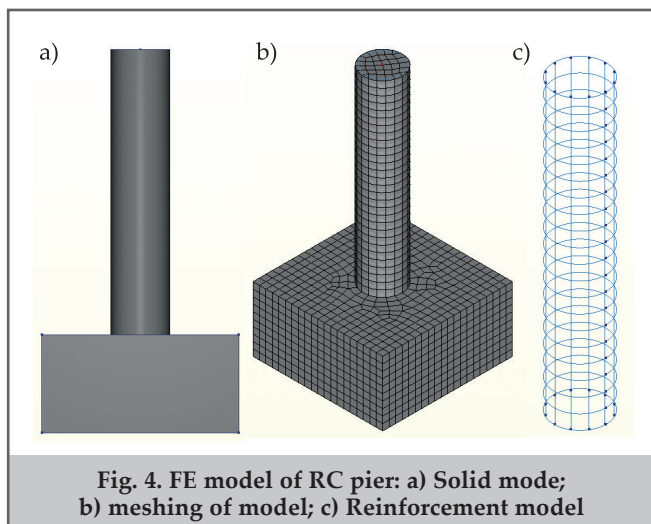


Fig. 4. FE model of RC pier: a) Solid mode; b) meshing of model; c) Reinforcement model

Internal force changing according different concrete class								Table 2
Concrete class	$f_c$ , mm	$P$ , kN	$\epsilon_b$	$x$ , m	$N_b$ , kN	$N_s$ , kN	$M_b$ , kNm	$M_s$ , kNm
B20	11.09	3982.8	0.0018	1.33	2931.9	1050.4	47.0	11.1
B30	11.68	5309.0	0.0018	1.26	4274.3	1034.7	76.1	11.68
B40	12.02	6512.9	0.0018	1.23	5487.3	1025.6	103.3	40.1

values, which means that higher-class concretes provide not only a higher load-bearing capacity but also better stability.

The analysis of the other structural parameters (table 2) such as bending moments revealed that going from B20 to B30 class concrete resulted in a gain of 62.4% in the capacity to resist bending moments, while going from B30 to B40 class concrete increased this capacity by another 35.8%. This confirms the benefits accruing from the use of superior-grade concrete when the need is to distribute the bending stresses more effectively.

As can be observed from the table, although an increase in the concrete class leads to an increase in the value of the compressive force perceived by the concrete in the section, the normal force perceived by the reinforcing bars remains almost unchanged. It should be noted that in the considered example, the increasing arm of the full deformation diagram of concrete in compression is realized until the moment of loss of the load-bearing capacity. For all three classes of concrete, the value of the concrete strain on the outer compressive face of the section with the highest stress now of loss of the load-bearing capacity was  $\epsilon_b=0.0018$ . When the loss of the load-bearing capacity, all reinforcements, except for the fourth reinforcement, worked within the elastic limit, but the fourth reinforcement reached the yield point. It should also be noted that an increase in the concrete class also increases the value of the element deflection at the critic moment.

Further detailed analysis was performed by monitoring the position of the neutral axis and internal force distribution within the section (fig. 6). The position of the neutral axis, represented by the parameter  $x$ , was examined with respect to the compressive strain  $\epsilon_b$  in the most stressed section of the compressed face. Indeed, it was observed that the class of concrete had a weak influence on this parameter. It does not change significantly by class of concrete the variation of  $x$  in terms of strain  $\epsilon_b$ , because it means that changes within deformation behavior occurred only around the compressed zone.

From a similar perspective, another parameter associated with the normal forces within concrete and steel reinforcements has also been addressed. For different classes of concrete, the internal compressive force exerted by the concrete increased with the class of concrete, whereas the forces borne by the reinforcing bars remained almost unaffected (fig. 7). This pattern reflects the increased contribution of concrete to the load-bearing capacity with increasing strength. It was observed that the compressive force in the concrete increased up to a certain strain level (in the examined case,  $\epsilon_b=0.0018$ ); above this value, it started to decrease, and the reduction occurred because some reinforcing bars had already reached their yield limit owing to the redistribution of the internal forces within the section.

The calculations also indicated that the value of the internal bending moment  $M_b$ , owing to the compressive stresses

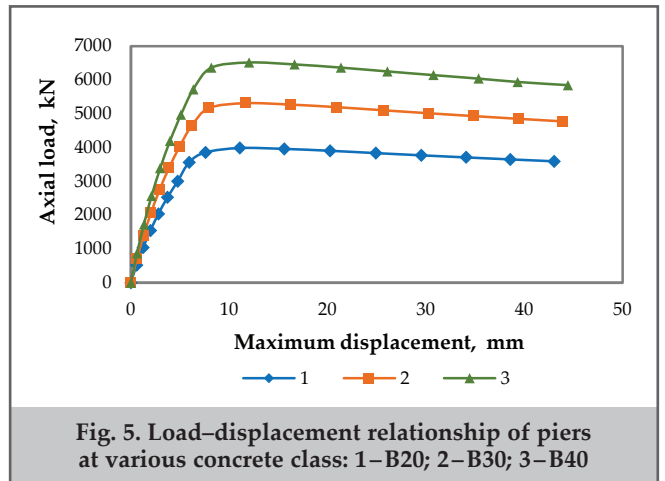


Fig. 5. Load-displacement relationship of piers at various concrete class: 1-B20; 2-B30; 3-B40

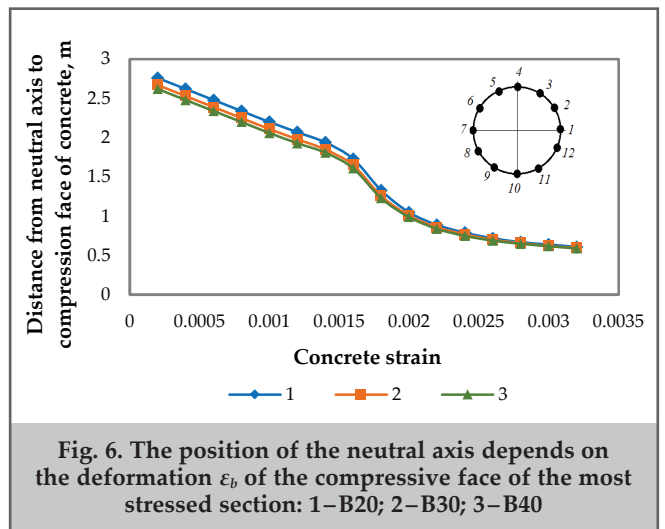


Fig. 6. The position of the neutral axis depends on the deformation  $\epsilon_b$  of the compressive face of the most stressed section: 1-B20; 2-B30; 3-B40

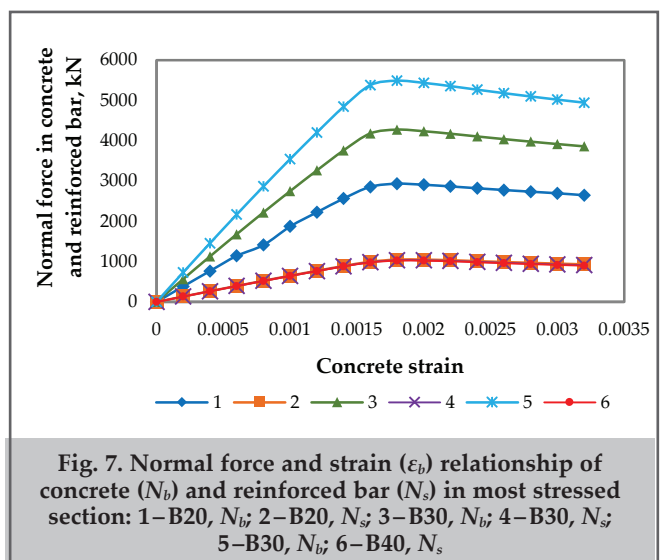
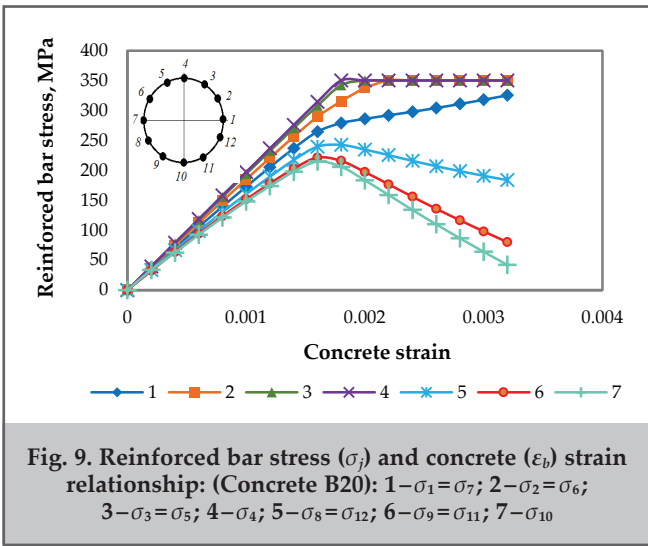
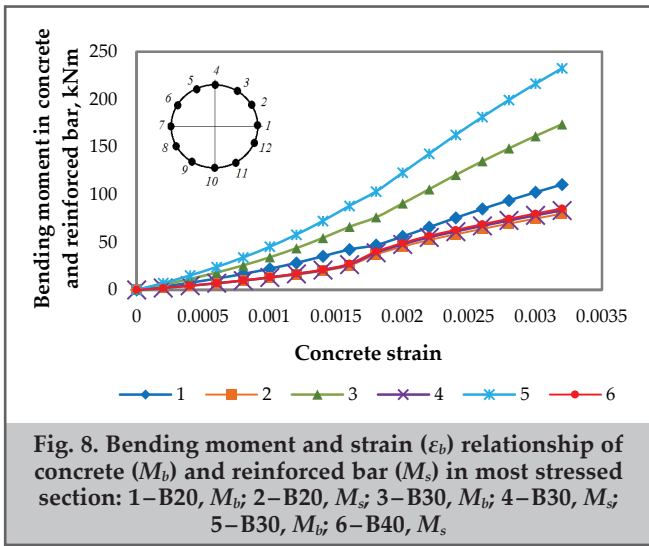


Fig. 7. Normal force and strain ( $\epsilon_b$ ) relationship of concrete ( $N_b$ ) and reinforced bar ( $N_s$ ) in most stressed section: 1-B20,  $N_b$ ; 2-B20,  $N_s$ ; 3-B30,  $N_b$ ; 4-B30,  $N_s$ ; 5-B30,  $N_b$ ; 6-B40,  $N_s$



in the concrete of the most stressed section of the assumed central compressed element, increases significantly with an increase in the class of the concrete (fig. 8). Unlike the internal normal force,  $M_b$  continued to increase until failure was achieved. Although the value of the normal force absorbed by the concrete increases up to a certain value of strain, a decrease in the normal force is observed after a certain value of strain. Somewhat parallel, the bending moment that is carried by normal stresses in the reinforcement bars proved insensitive to the specific value of the concrete class; similarly, this parameter monotonously increased up to the ultimate limit state and demonstrated the complementarity of the reinforcement in the structural response of the specimen. Here,  $M_s$  is independent of the concrete class, underscoring that the main resistance against an axial tensile force primarily comes from the reinforcement bars, while the role of concrete becomes increasingly dominant in managing compressive stresses and moments.

Figure 9 shows an elaborate view of the normal stress variation in the longitudinal reinforcement bars with respect to increasing  $\epsilon_b$  strain at the compressed face of the section. The variation patterns of these stresses were not the same for all reinforcement bars. The stress variation pattern for the second, third, and fourth reinforcement bars was almost linear until the yield limit was attained. The first reinforcement bar exhibited an increase in stress up to failure without attaining its yield limit. This trend is different from that demonstrated

by the eighth, ninth, and tenth reinforcement bars, whose stresses first increased to a certain value of deformation, after which they started declining. In specific terms, for instance, this scenario reflects in the eighth reinforcing bar with a rise of stress to  $\sigma_8=242.42$  MPa at  $\epsilon_b=0.0018$ , which lowers back down to  $\sigma_8=183.61$  MPa at  $\epsilon_b=0.0032$ , showing a decay trend. Again, in the ninth and tenth bars, the increased magnitude stress magnitudes at  $\epsilon_b=0.0016$  were at  $\sigma_9=221.25$  MPa and  $\sigma_{10}=214.56$  MPa, respectively, further reducing at the same magnitude of  $\epsilon_b=0.0032$  to  $\sigma_9=79.92$  MPa and  $\sigma_{10}=41.97$  MPa, correspondingly.

**5.2. Effect of pier heights on the structural performance of RC circular piers**

As a second parametric study, the impact of pier slenderness on the stress-strain state of the central compressed elements was examined. For this analysis, the initial parameters were kept constant, while the pier heights were varied as  $l=2$  m,  $l=3$  m, and  $l=4$  m. The results of these calculations are represented in the load-displacement curves in figure 10. The figure reveal that the slenderness of the compressed element significantly influences the load-displacement response. Specifically, as the pier height increased, the deformation corresponding to the maximum load on the load-displacement curve showed a sharp increase. With the increase in pier height, the pattern of load-carrying capability showed an apparent decrease. In the case, with  $l=2$  m, the bearing

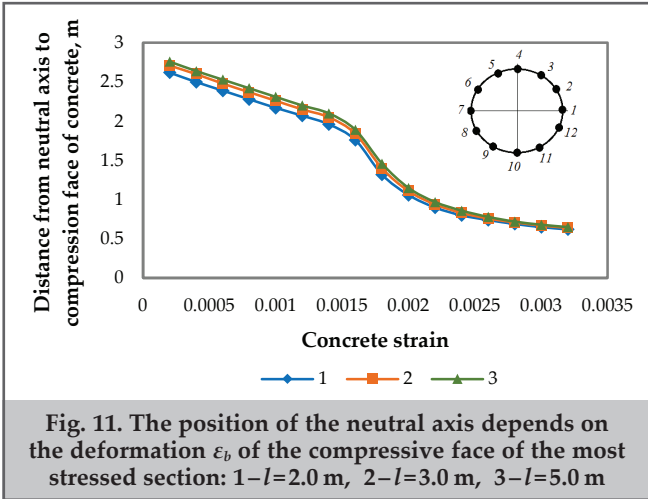
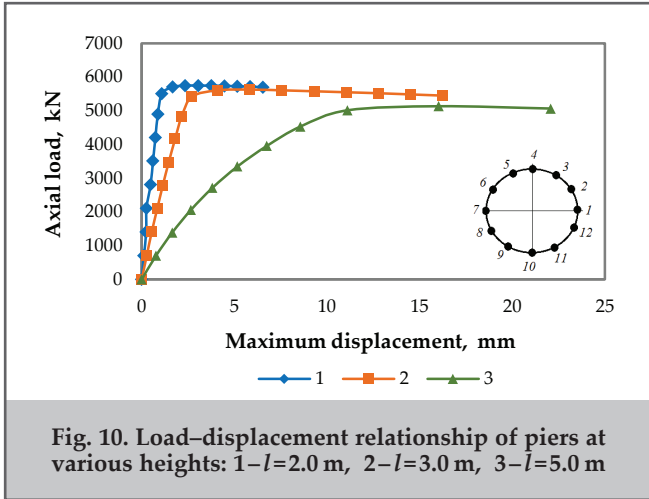


Table 3

Internal force changing according different slendress								
Pier height	$f$ , mm	$P$ , kN	$\epsilon_b$	$x$ , m	$N_b$ , kN	$N_s$ , kN	$M_b$ , kNm	$M_s$ , kNm
$l=2.0$ m	3.06	5750.8	0.0022	1.16	4602.5	1148.3	41.8	33.4
$l=3.0$ m	5.81	5632.5	0.0020	1.26	4515.8	1116.7	53.0	36.1
$l=5.0$ m	16.03	5138.2	0.0018	1.14	4139.2	999.1	90.3	43.1

capacity of the pier was estimated to be 5750.8 kN, whereas this value for  $l=3$  m fell to 5632.5 kN, that is, a reduction of approximately 2.1%. This makes the bearing capacity reached up to 5138.2 kN for an increased height of  $l=5$  m, in which the total reduction has gone to 10.6% against the  $l=2$  m pier.

The parameters characterizing the stress-strain state at the point of load-bearing capacity loss for each height configuration are listed in table 3. From the table, it is evident that as the pier height or slenderness increases, the deformation values at the compressed face of the most stressed section decrease. The calculations indicated that under critical conditions, the second, third, and fourth reinforcement bars in the  $l=2$  m pier reached their yield limits. In the case of the  $l=3$  m pier, the yielding limit was reached at the third and fourth bars, whereas in the case of the  $l=5$  m pier, only the fourth reinforcement bar reached its yield limit. These results indicate that a high pier slenderness significantly affects the structural performance of circular RC piers. A taller pier indicates less deformation in the compressed face and different distributions of stresses among the reinforcement bars; therefore, precise modeling and analysis are required to ensure that structural safety and performance can be guaranteed.

Figure 11 depicts the tendency of the change neutral axis position in the various height of the pier depending on the parameter  $x$  at the considered values of  $\epsilon_b$ . A comparison of the values shows that, as the flexibility of the pier increases, the regularity of the change in the parameter changes more uniform. This figure shows that the height of the compression zone of the section, which plays an important role in the calculation of reinforced concrete elements owing to the simplification of the real deformation diagram of the material, cannot be accurately determined. In the considered case, when studying the change in stresses in the reinforcement bars, it was determined that the nature of the change in these stresses is approximately the same as in figure 7.

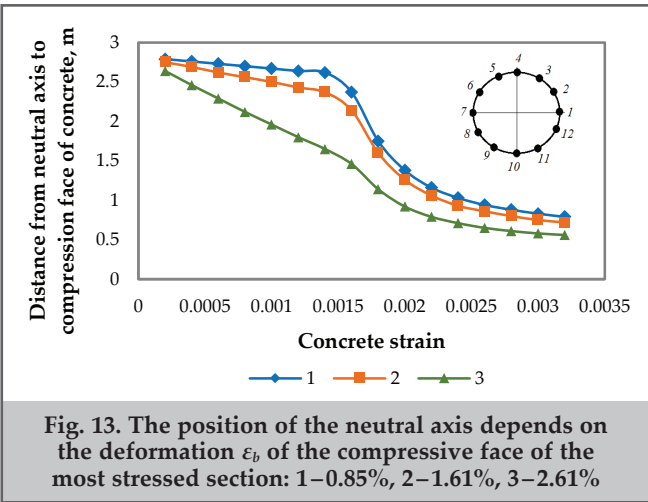
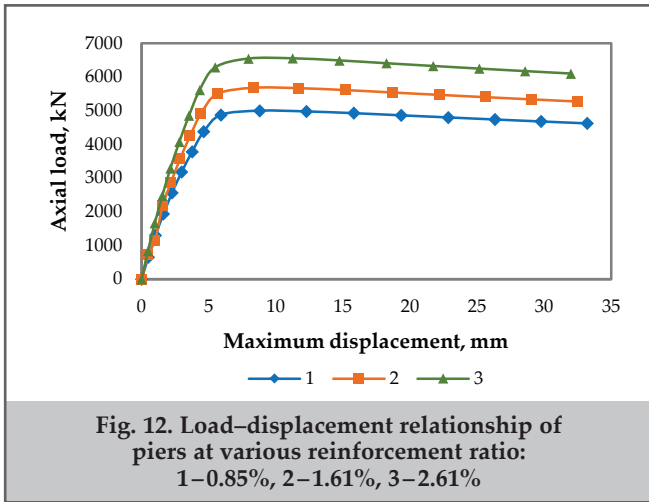
### 5.3. Effect of reinforcement ratio on the structural performance of RC circular piers

The third parametric study focused on the effect of the reinforcement ratio on the stress-strain state and load-bearing capacity of circular cross-section pier structures. For this analysis, the concrete class was fixed at B30, the pier height was set to  $l=4$  m, and the other geometric parameters remained unchanged. The element was reinforced with steel classes corresponding to  $A_s=24.13$  sm<sup>2</sup> (0.85%, 12Ø16),  $A_s=45.62$  sm<sup>2</sup> (1.61%, 12Ø22), and  $A_s=73.89$  sm<sup>2</sup> (2.61%, 12Ø28). The results of these calculations were illustrated in «load-displacement» curves presented in figure 12. The curves indicate that owing to the realization of descending branches, the load-bearing capacity of the pier is determined by the stability conditions. When the total reinforcement area increased from  $A_s=24.13$  sm<sup>2</sup> to  $A_s=45.62$  sm<sup>2</sup>, the critical load increased by 13.6%, rising from 4999 kN to 5678.6 kN. Further

increasing the reinforcement area to  $A_s=7389$  sm<sup>2</sup> resulted in a 31.1% increase in the critical load, reaching 6556.5 kN. Results demonstrate that the reinforcement ratio significantly affects the load-bearing capacity of compressed circular cross-sectional elements. The influence of the reinforcement percentage underscores the necessity of applying actual deformation diagrams of materials to ensure accurate calculations and optimize the design of RC structures.

The values of the parameters characterizing the stress-strain state in the event of a crisis are listed in table 4. These parameters are important for understanding the behavior of concrete and reinforcement, and assessing the forces to which they are exposed at critical moments. The change in the normal force and moment generated in the concrete and reinforcement with increasing reinforcement ratio clearly shows the effect of the reinforcement ratio on the overall stability and performance of the structure. According to the data given in table 4, when the reinforcement ratio was 0.85%, the normal force generated in the concrete of the pier was  $N_b=4237.6$  kN and the moment was  $M_b=70.3$  kNm. When the reinforcement percentage was 1.61%, the normal force of the concrete was  $N_b=4388.4$  kN ( $M_b=63.3$  kNm) and when the reinforcement percentage was 2.61%, the normal force was  $N_b=4417.5$  kN ( $M_b=66.9$  kNm). These results clearly demonstrate how the normal force and moment generated in the concrete and reinforcements change with an increasing reinforcement ratio. This trend shows that with the reinforcement ratio, the normal force of concrete increased by an average of 3.90%, while the change in moment was -7.40% on average. Based on the reinforcement percentages given in table 4, it is concluded that the increase in reinforcement percentage increases the normal force and moment generated in the reinforcements by an average of 65-75% in the critical case. This allows us to understand that the reinforcement percentage has a significant effect on the overall strength and stability of piers and how the structure behaves in a critical situation. However, an increased reinforcement ratio makes the structure more stable.

Figure 13 illustrates that the reinforcement ratio hardly affects the position of the neutral axis expressed by parameter  $x$ . For all three reinforcement cases, the variations in this parameter were qualitatively and quantitatively similar. However, there was a slight increase in  $x$  as the reinforcement ratio increased, especially in the initial stages of loading. The results from the analysis indicated that in the critical state, for the first two reinforcement configurations, only the fourth reinforcement bar reached its yield limit, whereas in the case of the third reinforcement configuration, the third and fourth reinforcement bars reached their yield limits. These conclusions underline the fact that a small reinforcement ratio variation would be marginally influential in changing the position of the neutral axis but becomes important when deciding on the critical stress and yielding of the reinforcement bars.



Reinforcement ratio	$f$ , mm	$P$ , kN	$\epsilon_b$	$x$ , m	$N_b$ , kN	$N_s$ , kN	$M_b$ , kNm	$M_s$ , kNm
0.85 %	8.81	4999.0	0.0018	1.32	4237.6	671.4	70.3	23.8
1.61 %	8.33	5678.6	0.0018	1.40	4388.4	1290.2	63.3	40.8
2.61 %	11.26	6553.5	0.0020	1.15	4417.5	2136.0	66.9	72.4

5.4. FE verification

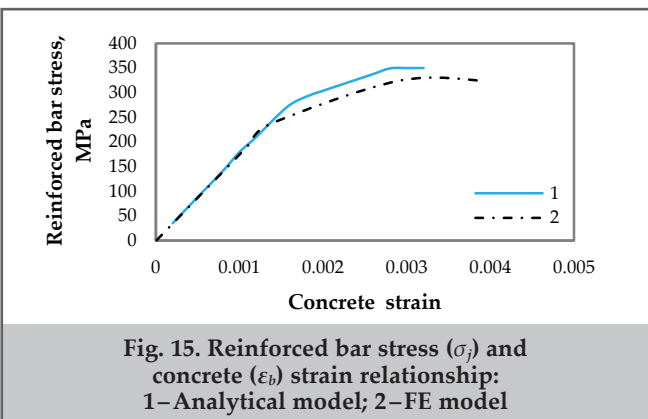
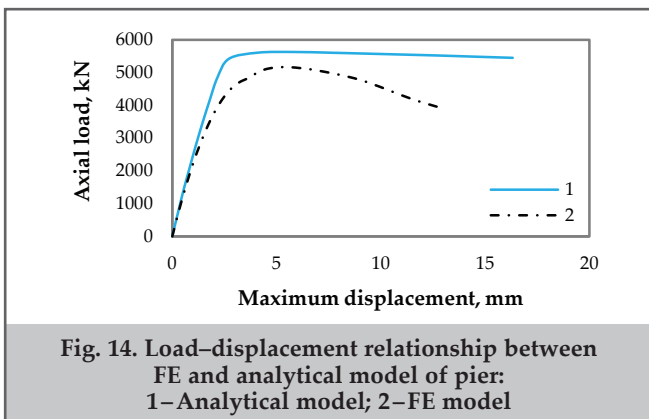
In this study, the developed analytical formulation for the performance analysis of RC piers was verified using DIANA FEA. Representative cases for evaluation were considered to be one pier with a height of 3 m. A comparison of the finite element model with the analytical model showed consistency to a large extent, which justified the developed approach.

Figure 14 shows that the load-displacement relationship shows very good agreement between the results obtained from both the analytical and FEM models. Meanwhile, the maximum axial load according to the analytical model was approximately 5632.5 kN, whereas according to the FEM, it was approximately 5110.4 kN, which is less than the difference of approximately 9.3% over the analytical model. The degree of agreement confirmed the correctness of the analytical formulations when interpreting the nonlinear load-displacement response in an RC pier. In addition, the proximity between the curves obtained in the entire loading range confirms the capability of the analytical model to simulate different structural responses, including elastic and inelastic stages.

The reinforced bar stress and concrete strain relationship

for the analytical and FE models were compared, as shown in figure 15. From the FEM, the maximum value in the stress of the reinforcement was 350 MPa; from the analytical model, the peak value in the reinforcement was 345 MPa. The deviation in the peak values of the FEM from the analytical model was the two models indicated excellent agreement, within a deviation of less than 2%. These results are used to validate the capability of the analytical formulations to capture the localized stress and strain distributions in the pier with high accuracy, which is of paramount importance in assessing its performance under axial and bending loads.

The results validate the analytical formulations developed in this study as reliable and robust for predicting the structural behavior of RC piers. The presented results demonstrate the robustness of the adopted analytical model as well as its validity for application to practical engineering problems. Furthermore, the analytical and finite element solutions presented prove the adequacy of the proposed formulation for performing parameter studies and performance evaluations of RC piers. These highlight the application of analytical techniques in tandem with finite element approaches in such studies.



## Conclusions

The objective of this study is to analyze the structural performance of circular RC piers by considering a large number of parameters. This study presents an innovative analytical solution for the design and performance evaluation of an RC circular pier validated by FE modeling. The major results of this study are summarized as follows.

- The concrete class has a significant influence; increasing the class of concrete increases the bending moment. Thus, it can be inferred that high-strength concrete plays a crucial role in enhancing the load-bearing capacity of RC piers. In addition to such significant improvements in the load-bearing capacity, the shifting of the neutral axis occurred within very limited variations, which underlines, among other things, how increased rigidity and the increase in resistance to bending were governed essentially by concrete strength rather than geometric effects.
- Effectiveness of pier height an inversely proportional relation derived between pier height and load-bearing capacity gave, for a pier of taller height, a reduction of up to 10.6% in the values of critical load. Larger slenderness ratios increase the possibility of buckling; therefore, prudent proportioning of height to width at the design stage with respect to stability and safety considerations was in order.
- The reinforcement ratio is an important parameter that influences the load-bearing capacity. For increased reinforcement ratios, the critical load value increased in all the cases. Whereas the position of the neutral axis practically did not change, for a higher reinforcement ratio, a strong redistribution of stresses within the reinforcement bars was achieved; thus, the structural performance under loading conditions improved.
- The FE model presented a very good validation of the proposed analytical formulations, while discrepancies in the load predictions and stress-strain responses remained below 10%. This excellent agreement between the numerical and analytical results proves the reliability of the developed methodologies; thus, they are applicable for practice and further research.
- An integrated design approach using both analytical and numerical methods is underlined with respect to the optimization of the design parameters of RC piers. The present research, therefore, provides comprehensive guidelines that would aid engineers and researchers in understanding how to handle the problem of design and evaluation difficulties of RC piers, which would directly contribute to improving the safety, efficiency, and cost-effectiveness of construction methods.

## References

1. Vadluga, R., Kliukas, R., (2012). The use of annular and circular cross-section members in transport and power engineering building construction. *The Baltic Journal of Road and Bridge Engineering*, 7 (2), 77–83.
2. Di Laora, R., Galasso, C., Mylonakis, G., et al. (2020). A simple method for N-M interaction diagrams of circular reinforced concrete cross sections. *Structural Concrete*, 21 (1), 21–55.
3. Gu, X. L., Jin, X. Y., Zhou, Y., (2016). Basic principles of concrete structures. *Springer Verlag, Berlin Heidelberg & Tongji University Press*.
4. Yang, Y. S., Yang, C. M. (2015). Thin crack observation in a reinforced concrete bridge pier test using image processing and analysis. *Advances in Engineering Software*, 83, 99–108.
5. Sha, Y., Hao, H. (2013). Laboratory tests and numerical simulations of barge impact on circular reinforced concrete piers. *Engineering Structures*, 46, 593–605.
6. Su, J., Wang, J., Li, Z., et al. (2019). Effect of reinforcement grade and concrete strength on seismic performance of reinforced concrete bridge piers. *Engineering Structures*, 198, 109512.
7. Dundu, M. (2012). Compressive strength of circular concrete filled steel tube columns. *Thin-Walled Structures*, 56, 62–70.
8. Cheon, J.-H., Kim, T. H., Lee, B. J., et al. (2012). Inelastic behavior and ductility capacity of circular hollow reinforced concrete bridge piers under earthquake. *Magazine of Concrete Research*, 64(10), 919–930.
9. Karim, H., Sheikh, M. N., Hadi, M. N. S. (2016). Axial load-axial deformation behavior of circular concrete columns reinforced with GFRP bars and helices. *Construction and Building Materials*, 112, 1147–1157.
10. Akiyama, M., Matsuzaki, H., Dang, H. T., Suzuki, M. (2012). Reliability-based capacity design for reinforced concrete bridge structures. *Structure and Infrastructure Engineering*, 8(12), 1096–1107.
11. Pham, T. M., Doan, L. V., Hadi, M. N. S. (2013). Strengthening square reinforced concrete columns by circularization and FRP confinement. *Construction and Building Materials*, 48, 19–24.
12. Li, B., Zohrevand, P., Mirmiran, A. (2013). Cyclic behavior of FRP concrete bridge pier frames. *Journal of Bridge Engineering*, 18(5).
13. Zhang, X., Zhang, H. (2014). Axial crushing of circular multi-cell columns. *International Journal of Impact Engineering*, 65, 110–125.
14. Uenaka, K., Kitoh, H., Sonoda, K. (2010). Concrete filled double skin circular stub columns under compression. *Thin-Walled Structures*, 48, 19–24.

15. Zeng, J. J., Guo, Y. C., Gao, W. Y., et al. (2018). Stress-strain behavior of concrete in circular concrete columns partially wrapped with FRP strips. *Composite Structures*, 200, 810–828.
16. Fahmy, M. F. M., Wu, Z. (2010). Evaluating and proposing models of circular concrete columns confined with different FRP composites. *Composites: Part B*, 41, 199–213.
17. Hadi, M. N. S., Karim, H. F., Sheikh, M. N. S. (2016). Experimental investigations on circular concrete columns reinforced with GFRP bars and helices under different loading conditions. *Journal of Composites for Construction*, 20(4), 04016009.
18. Gadjiyev, M. A., Guseynov, I. G., Gadjiyeva, U. M. (2023). Stress-strain state and load ability of compressed pipe-concrete elements. *SOCAR Proceedings*, 9(2), 21–26.
19. Hajiyev, M. A., Damirov, M. M. (2023). Stress-strain state and bearing capacity of compressed reinforced concrete elements of annular section. *Architectural Studies*, 9(2), 35–46.
20. Hajiyev, M. A., Damirov, M.M. (2024). Construction of the «Moment-Curvature» scheme for annular cross-sectional reinforced concrete elements and its application in the calculation of reinforced concrete beams. *HERALD of the Azerbaijan Engineering Academy*, 16(1), 56–69.
21. Hajiyeva, U. M. (2021). Calculation of compressed reinforced concrete elements with a circular cross section according to a nonlinear deformation model. *Expert: Theory and Practice*, 5(14)), 13-20.
22. Hajiyeva, U. M. (2020). Calculation of a compressed reinforced concrete element with a circular cross section using a three time concrete compression scheme. In: *The 3rd International Conference on Building Innovations*, Springer International Publishing.
23. Hajiyeva, U. M. (2021). Stress deformation state and load-bearing capacity of circular cross-sectional compressed reinforced concrete elements based on two-line diagrams of materials. *Construction and Architecture in Azerbaijan*, 3, 9–15.
24. Pavlikov, A., Kochkarev, D., Harkava, O. (2019). Analysis of eccentrically loaded members of circular cross section by nonlinear deformation model. In: *International Conference Building Innovations*. Cham: Springer International Publishing.
25. Kodysh, E. N., Nikitin, I. K., Trekin, N. N. (2010). Calculation of reinforced concrete structures of heavy concrete on strength, cracking and deformations. Monograph. Moscow: Association of Construction Universities.
26. Kolmogorov, A. G., Plevkov, V. S. (2014). Calculation of reinforced concrete structures according to Russian and foreign norms. Moscow: ASV.
27. Krishan, A. L., Krishan, M. A. (2014). Influence of flexibility on bearing capacity of compressed reinforced concrete elements. *Khabarovsk: Pacific State University*.
28. Murashkin, G. V., Mordovsky, S. S. (2013). Application of deformation diagrams for calculation of load-bearing capacity of off-centre compressed reinforced concrete elements. *Housing Construction*, 3, 38–40.
29. Rimshin, V. I., Krishan, A. L., Mukhametzyanov, A. I. (2015). Constructing a deformation diagram of uniaxially compressed concrete. *Proceedings of Moscow State University of Civil Engineering*, 6, 23-31.
30. Starishko, I. N. (2014). Methods for determining the carrying capacity of eccentrically compressed concrete elements. *Proceedings of Moscow State University of Civil Engineering*, 4, 59–69.
31. SP 63.13330.2018. (2018). Concrete and reinforced concrete structures. General provisions. Moscow: JSC SIC Construction. A.A. Gvozdev NIIZhB.
32. Ferreira, D., Manie, J. (2022). DIANA - Finite element analysis: DIANA Documentation - Release 10.4. DIANA FEA BV.
33. Ferreira, D. (2013) A model for the nonlinear, time-dependent and strengthening analysis of shear critical frame concrete structures. Doctoral Thesis. *Universitat Politècnica de Catalunya*.
34. Bashirzade, S., Ozcan, O., Cagdas, I. U. (2024). Internal force transfer in segmental RC structures. *Research on Engineering Structures & Materials*, 10(4), 1639-1662.
35. Chai, S. (2020) Finite element analysis for civil engineering with DIANA software. Singapore: Springer Nature.
36. Bashirzade, S. R., Lipin, A. A., Hajiyev, M. A., et al. (2024). Fire resistance of offshore concrete structures. *SOCAR Proceedings*, 4, 79-84.
37. Aslanov, L. F., Aslanlı, U. L. (2024). Study of marine hydraulic structures under seismic effects. In: Ksibi, M., et al. Recent advances in environmental science from the Euro-Mediterranean and surrounding regions. EMCEI 2022. Advances in Science, Technology & Innovation. Springer, Cham.